Journal of Magnetic Resonance 194 (2008) 156–161

Contents lists available at ScienceDirect

Journal of Magnetic Resonance

journal homepage: www.elsevier.com/locate/jmr

Communication

# Rapid encoding of $T_1$ with spectral resolution in $n$-dimensional relaxation correlations

T.C. Chandrasekera [a], J. Mitchell [a], E.J. Fordham [b], L.F. Gladden [a], M.L. Johns [a,*]

[a] Department of Chemical Engineering, University of Cambridge, Pembroke Street, Cambridge, Cambridgeshire CB2 3RA, United Kingdom
[b] Schlumberger Cambridge Research, High Cross, Madingley Road, Cambridge CB3 0HG, United Kingdom

ARTICLE INFO

*Article history:*
Received 28 March 2008
Revised 7 June 2008
Available online 24 June 2008

*Keywords:*
Relaxation correlations
Relaxation exchange
Laplace inversions
Broad line samples
Porous media
Permeable rocks
Cellulose fibres

ABSTRACT

Nuclear magnetic resonance (NMR) $T_1$ relaxation times have been encoded in the second dimension of two-dimensional relaxation correlation and exchange experiments using a rapid "double-shot" $T_1$ pulse sequence. This technique also retains chemical shift information ($\delta$) for short $T_2^*$ materials. In this way, a spectral dimension can be incorporated into a $T_2$–$T_1$–$\delta$ correlation without an increase in experimental time compared to the conventional, chemically insensitive $T_1$–$T_2$ correlation. Here, the $T_2$–$T_1$–$\delta$ pulse sequence is used to unambiguously identify oil and water fractions in a permeable rock. A novel $T_1$–$T_1$–($\delta$) relaxation exchange measurement is also introduced and used to observe diffusive exchange of water in cellulose fibres.



## 1. Introduction

Nuclear magnetic resonance (NMR) $T_2$ relaxation times have been used extensively in multi-dimensional relaxation measurements of porous media [1,2]. This is facilitated by the ease and efficiency of acquiring transverse relaxation decays using single-shot Carr–Purcell–Meiboom–Gill (CPMG) echo trains [3,4], although these rapid $T_2$ measurements lack spectral resolution and can be influenced by magnetic susceptibility induced gradients. The speed of the $T_2$ measurement can outweigh the disadvantages for favourable samples in low-field measurements ($B_0 < 1$ T), where chemical shifts are often less than the inherent line width of the systems, and enhanced relaxation due to magnetic susceptibility induced gradients can be neglected. However, when using high-field magnets it is desirable to retain spectral resolution, and for porous media studies it is essential to avoid the detrimental influence of the inherent internal gradients. If samples contain large quantities of paramagnetic impurities, these internal gradients can be significant even at low magnetic field strengths. We address these points by demonstrating the use of a fast, "double-shot" method for encoding $T_1$ whilst retaining spectral resolution in multi-dimensional relaxation measurements. The experimental time scale of the double-shot pulse sequence is similar to that of a CPMG measurement.

$T_1$–$T_2$ correlation plots are useful in determining the ratio $T_1/T_2$ as a characteristic parameter for permeable rocks [1]. However, the presence of both oil and water can complicate the analysis. Reservoir rocks are therefore usually analysed using $D-T_2$ correlations [5] because of the distinct difference in $D$ of the fluids [6,7]. In the $T_2$–$T_1$–$\delta$ correlations presented here, the chemical shifts ($\delta$) allow the signal from oil and water to be unambiguously distinguished. Chemically resolved $T_1$–$T_2$ correlations are possible [8,9], although due to the necessity of acquiring individual echoes in the CPMG train they are more time consuming by a factor of $n$ than the $T_2$–$T_1$–$\delta$ measurement presented here, where $n$ is the number of data points in the $T_2$ dimension.

$T_2$–$T_2$ exchange measurements have been used to observe the diffusive exchange between different regions of porosity in rocks [2] and cement pastes [10]. This method is also applicable to observing exchange between different chemical environments due to enhanced relaxation in magnetic susceptibility induced gradients, as was demonstrated in packed beds of glass spheres [11]. In chemically complex porous samples, or for high-field measurements, enhanced relaxation mechanisms (e.g., exchange or magnetic field gradients) can be difficult to distinguish. Novel $T_1$–$T_1$–($\delta$) measurements offer a method of observing pore-to-pore exchange without the influence of such internal gradients due to magnetic susceptibility differences, and inherently include spectral resolution. Here, $T_1$–$T_1$–($\delta$) and $T_2$–$T_2$ measurements are used to determine the exchange rate of water moving between cellulose fibres; since we are observing only water, the spectral

* Corresponding author.
*E-mail address:* mlj21@cam.ac.uk (M.L. Johns).

1090-7807/$ - see front matter © 2008 Elsevier Inc. All rights reserved.
doi:10.1016/j.jmr.2008.06.008

dimension of the $T_1$–$T_1$–($\delta$) experiment does not contain any useful information in this case. Both methods are seen to provide similar exchange rates, although the $T_1$–$T_1$–($\delta$) plots contain discrete peaks, simplifying the analysis.

Several rapid $T_1$ measurements have been proposed previously, including the Look and Locker sequence [12]—also known as $T_1$ by multiple read-out pulses (TOMROPs) [13]—and the triplet sequence [14]. These techniques have, for the most part, been used to determine single relaxation time components or to add $T_1$ weighting to magnetic resonance imaging (MRI) experiments; a list of relevant publications can be found in [15]. Other rapid $T_1$ measurements have been proposed for use specifically in the strong magnetic field gradients of unilateral magnets, see for example [16]. The TOMROP sequence drives the longitudinal magnetisation to some arbitrary equilibrium level using small spin tip angle pulses. The data obtained are then a complicated function of the initial magnetisation $M_0$, the final equilibrium magnetisation $M_\infty^{eq}$, and the tip angle $\alpha$.

It is possible to remove the recovery to equilibrium leaving only an exponential decay [17]. Hsu and Lowe showed the TOMROP pulse sequence could be modified in this way for use in MRI $T_1$ mapping [18]. Here we apply this pulse sequence to the quantitative measurement of relaxation time distributions. In the modified TOMROP pulse sequence, phase cycling of an initial $z$-store pulse alternates the starting magnetisation from $+M_0$ to $-M_0$ on two successive scans, removing the equilibrium magnetisation component $M_\infty^{eq}$. The $T_1$ relaxation time is thereby encoded in an exponential decay of the form

$$M\{(n-1)\tau_1\} = 2M_0(\exp(-\tau_1/T_1)\cos\alpha)^{n-1}\sin\alpha, \quad (1)$$

where $\tau_1$ is the inter-$\alpha$ pulse delay. The constant term ($2M_0\sin\alpha$) only affects the initial observed magnetisation and not the $T_1$ relaxation time; the factor 2 results from the summation of two successive scans. If, for example, $\alpha = 5^\circ$ then after the first pulse, $n = 1$, the observed magnetisation will be $M\{0\} \approx 0.1743M_0$. After the second pulse, $n = 2$, the observed magnetisation will be $M\{\tau_1\} \approx 0.1736M_0\exp(-\tau_1/T_1)$. As $n \to \infty$, $M\{\infty\} \to 0$. We classify this sequence as a "double-shot" $T_1$ measurement due to the two scans necessary to alternate the direction of the $z$-store. This pulse sequence is similar to Difftrain [19] albeit without the bipolar field gradient pulses. Distributions of $T_1$ relaxation times from the double-shot measurement are verified here against those obtained from the conventional inversion recovery pulse sequence [20] by observing the longitudinal relaxation of water with varying concentrations of gadolinium dopant.

## 2. Experimental

The double-shot $T_1$ pulse sequence is shown in Fig. 1(a). The $\pm z$-store is generated by appropriate phase cycling of the $[90_x - 180_y - 90_{\pm x}]$ preparation pulses. This is followed by a train of $n$ small tip angle $\alpha$ pulses. After each $\alpha$ pulse, a free induction decay (FID) [21] is acquired, from which the chemical shift information is obtained. Homospoils are used to dephase any remaining coherent transverse magnetisation prior to the application of the next $\alpha$ pulse. The $T_2$–$T_1$–$\delta$ pulse sequence, Fig. 1(b), is created simply by repetition of the 180° pulse in the preparation portion of the double-shot sequence. In this way, $T_2$ is encoded in a CPMG train of $m$ echoes. The full data set is constructed by varying $m$ in successive acquisitions. The $T_1$–$T_1$–($\delta$) pulse sequence, Fig. 1(c), requires the addition of an initial inversion (or saturation) pulse, followed by a recovery delay $T_{RD}$, to encode $T_1$ in the first dimension. Exchange is observed across the preparation portion of the double-shot sequence between the two $T_1$ measurements. The magnetisation remains in the $x$–$y$ plane for a time $t_{ex} = 2m\tau_2$; over this time

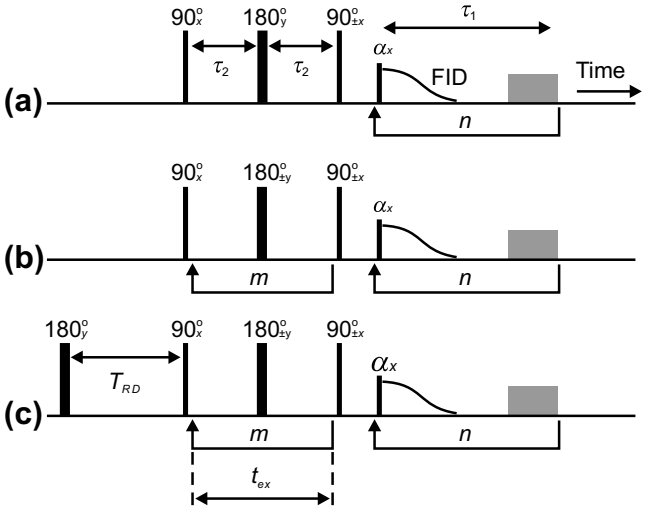


**Fig. 1.** (a) The double-shot $T_1$ pulse sequence. The first small tip angle $\alpha$ RF pulse immediately follows the $90^\circ_{\pm x}$ $z$-store pulse. The $\alpha$ pulse is repeated $n$ times and a FID is recorded after each pulse. The grey rectangles represent optional homospoils. (b) The $T_2$–$T_1$–$\delta$ pulse sequence where the 180° pulse is repeated $m$ times to generate a CPMG echo train. (c) The $T_1$–$T_1$–($\delta$) sequence has an initial inversion pulse followed by a variable recovery delay $T_{RD}$. Exchange is observed across the time interval $t_{ex} = 2m\tau_2$.

$T_2$ relaxation occurs. The exchange interval is varied by adjusting the number ($m$) of 180° pulses. It is necessary to encode the exchange across a series of spin echoes with $T_2$ weighting since a stimulated echo (as used in the $T_2$–$T_2$ exchange measurement [2]) would introduce a third longitudinal recovery interval. Three such consecutive recovery intervals would either cancel or enhance the $T_1$ weighting (depending on the phase cycle) and therefore would not provide a meaningful correlation between the two encoding portions of the pulse sequence.

The signal-to-noise (S/N) ratio is reduced in the double-shot $T_1$ measurement, compared to conventional $T_1$ techniques, due to the use of small tip angle pulses. In the experiments demonstrated here, the S/N ratio was sufficient for a large number of data points to be acquired. However, if the S/N ratio were lower, a larger tip angle could be used with fewer data points collected.

All the experiments were conducted on a 2 T (85 MHz $^1$H) horizontal imaging magnet controlled via a Bruker AV spectrometer. In all implementations of the double-shot $T_1$ measurement described here, the 90° and 180° pulse durations were $t_{90} = 15$ μs and $t_{180} = 30$ μs. The $\alpha$ pulses had a duration of $t_\alpha = 15$ μs but the pulse power was adjusted to provide $\alpha \approx 5^\circ$.

In the doped water samples, the concentrations of gadolinium (III) chloride were 0.1362, 0.01362, and 0 g L$^{-1}$, to provide approximate relaxation times of $T_1 = 40$, 300, and 3 s. For these double-shot $T_1$ measurements, $\tau_1 = 30$ ms (including a 5 ms homospoil) and $\tau_2 = 500$ μs. The total experiment time, acquiring $n = 256$ data points with eight scans, was 3 min. A conventional inversion recovery measurement, obtained with only 128 data points whose recovery delays were spaced logarithmically between $T_{RD} = 1$ and 15 s, and with four scans, lasted in excess of 2 h. These one-dimensional data sets were inverted using a Laplace transform algorithm based on the work of Wilson [22]. This algorithm inverts a Fredholm integral of the first kind with an appropriate exponential form to match the data being processed. The optimum smoothing (regularisation) parameter was chosen from the minimum in the generalised cross validation (GCV) curve. The GCV method determines the variation in the fit error when individual raw data points are removed from the fitting process and predicted by extrapolation of the fit to the remaining points.

The $T_2$–$T_1$–$\delta$ pulse sequence was applied to the identification of oil and water fractions in a permeable rock. The rock sample was a Bentheimer sandstone core with dimensions 70 mm × 38 mm (length × diameter). The core was vacuum saturated initially with 2 wt% KCl brine solution to prevent osmotic swelling of the clay content. Dodecane was pumped through the core to provide a binary saturation of oil and water. $T_2$ was encoded in the first dimension of the $T_2$–$T_1$–$\delta$ measurement by varying the number of even echoes from $m/2 = 1$ to 512 in 128 logrithmically spaced steps with $2\tau_2 = 1$ ms. $T_1$ was encoded in the second dimension using the double shot sequence with $\tau_1 = 50$ ms, $n = 128$ data points, and 16 scans. The total experimental time was 6 h. A conventional $T_1$–$T_2$ measurment (using inversion recovery to acquire the $T_1$ dimension) with 128 logarithmically spaced $T_1$ recovery intervals in the range $T_{RD} = 10$ ms to 15 s, and CPMG echo trains of $m/2 = 512$ even echoes with $2\tau_{CPMG} = 1$ ms, also lasted 6 h, although this measurement does not retain spectral resolution. To obtain a conventional $T_1$–$T_2$ data set with spectral resolution and an equivalent data density to the $T_2$–$T_1$–$\delta$ measurement described here would require 32 days.

For the exchange experiments, woven cellulose fibres were soaked in water and then drained to remove the excess bulk liquid. In the $T_1$–$T_1$–$(\delta)$ measurements, the first dimension consisted of 128 logarithmically spaced $T_1$ recovery delays in the range $T_{RD} = 10$ ms to 15 s. Exchange intervals of $t_{ex} = 1$, 2, 8, 32, 64, 128, and 256 ms were used. In the second $T_1$ dimension (the double-shot pulse sequence), $\tau_1 = 30$ ms and $n = 256$ data points. The average duration of a $T_1$–$T_1$–$(\delta)$ measurement, with eight scans, was 5 h; the precise time of each experiment was defined by the variable exchange interval. If a $T_1$–$T_1$–$(\delta)$ exchange measurement were acquired with the same data density but without using the double-shot $T_1$ measurement, it would have an average duration of 12 days.

To compare and validate the $T_1$–$T_1$–$(\delta)$ experiments, $T_2$–$T_2$ exchange correlations [2,10] were performed on the same cellulose fibres. The $T_2$–$T_2$ pulse sequence also consists of three distinct time intervals: the spins are encoded with $T_2$ weighting via a CPMG train with a variable number of echoes in the first interval. The spins are then $z$-stored for a defined exchange (storage) time $t_{ex}$ in the second interval, during which time the spins recover with $T_1$. The signal intensity is recorded during the third interval by acquiring a fixed number of echoes in another CPMG train. Here, the echo spacing was $\tau_{CPMG} = 1$ ms in both CPMG trains. The number of echoes in the first train was varied logarithmically between $m = 2$ and 1024 echoes; 512 even echoes were acquired in the second train. The exchange time was varied between $t_{ex} = 10$ ms and 1 s across six separate experiments.

A fast multi-dimensional Laplace transform algorithm [23] was used to invert all the two-dimensional relaxation data sets. This provides a stable solution (the fit error is on the same order as the noise variance) to the ill-posed inverse problem where the two-dimensional data set is reduced to the form of a linear Fredholm integral of the first kind. To compute the solution on a desktop computer, the data is compressed using single value decompositions (SVDs) of the appropriate kernel functions describing the exponential nature of the data dimensions. The optimum regularisation parameter was determined using the Butler, Reed, and Dawson (BRD) method [24].

## 3. Results and Discussion

One-dimensional distributions of $T_1$ relaxation times can be seen in Fig. 2 for the doped water samples determined using (a) the conventional inversion recovery measurement and (b) the rapid double-shot measurement. The inserts show the curve fits to the raw data. The $T_1$ distributions are similar in each case: modal relaxation times of $T_1 \approx 45$ ms, 310 ms, and 2.78 s are obtained. The peaks are narrower in Fig. 2(b), compared to Fig. 2(a), because more data points were used in the inversion.

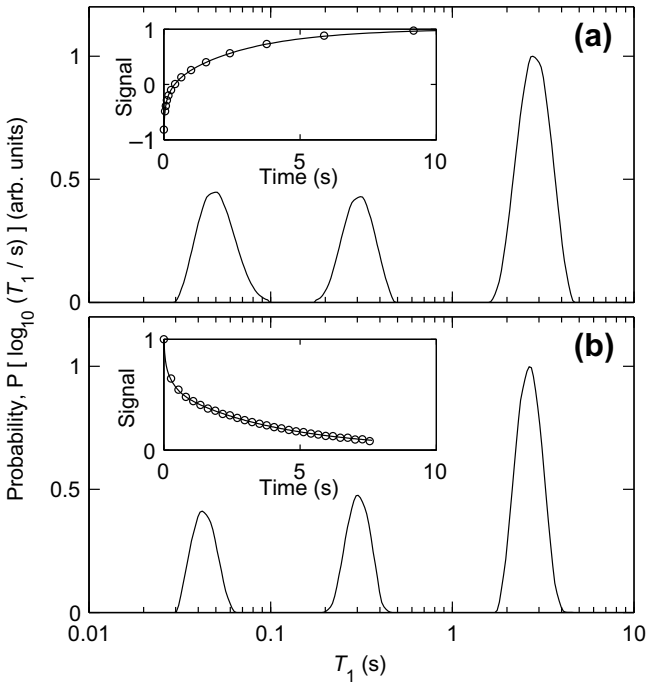


**Fig. 2.** $T_1$ relaxation time distributions (normalised to the maximum peak intensity) obtained from (a) inversion recovery and (b) double-shot measurements of three doped water samples. The inserts show the normalised signal (in arbitrary units) obtained from each sequence; the solid lines represent the multi-component fits to the data.

A conventional $T_1$–$T_2$ correlation is shown in Fig. 3(a) for the sandstone core saturated with dodecane (oil) and brine solution (water). Three distinct peaks are visible in the plot, although without *a priori* knowledge of the relaxation behaviour for the oil and water in the rock porosity, it is difficult to associate the peaks to the two liquids reliably. The equivalent $T_2$–$T_1$–$\delta$ measurement is shown in Fig. 3, resolved spectrally into the (b) oil and (c) water fractions; a typical spectrum can be seen in Fig. 3(d) showing the resolved water ($\delta = 4.69$ ppm) and oil ($\delta \approx 1$ ppm) signals. From the position of the peaks in the $T_2$–$T_1$–$\delta$ plots, it can be seen that the water is in contact with the pore walls (since the peaks lie on the frequency dependent diagonal line $T_1 = 8T_2$ [25]). The oil, exhibiting a single peak centred on $T_1 = 1$ s and $T_2 = 0.6$ s, may reside in the larger pores, or in the centre of the pores surrounded by a layer of water. The possibility of separating oil and water signals in $T_2$–$T_1$–$\delta$ correlations within a reasonable experimental time could provide a method for examining surface interactions in mixed wettability cores.

Examples of $T_1$–$T_1$–$(\delta)$ exchange plots for water in cellulose fibres can be seen in Fig. 4 for exchange intervals of (a) $t_{ex} = 2$, (b) 32, and (c) 128 ms. Two spin reservoirs are present associated with water in two pore sizes [26], assumed to be the internal fibre porosity and porous voids between fibre layers, with characteristic longitudinal relaxation times of $T_1 = 0.19$ s and $T_1 = 1.37$ s, respectively. The reservoir with a short $T_1$ is not observed in the two-dimensional plots because of rapid $T_2$ relaxation resulting in significant signal loss during the exchange interval. Exchange peaks are observed even in the case of the shortest possible exchange time, $t_{ex} = 2$ ms, because diffusive exchange occurs during the initial $T_1$ encoding portion of the pulse

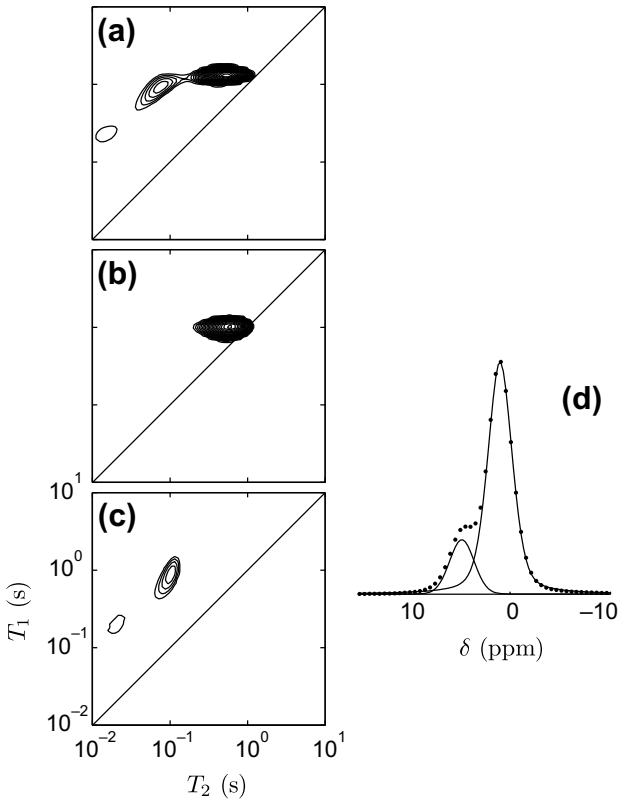


**Fig. 3.** Relaxation correlation measurements of a sandstone rock saturated with oil and water obtained from (a) the conventional $T_1$–$T_2$ correlation and (b,c) the $T_2$–$T_1$–$\delta$ correlation allows the signal from the (b) oil and (c) water fractions to be resolved. The contour intervals are the same in each plot. (d) A typical spectrum from the last dimension of the $T_2$–$T_1$–$\delta$ data set is shown (dotted line) from which the water ($\delta = 4.69$ ppm) and oil ($CH_2$, referenced to $\delta = 1.27$ ppm) fractions can be resolved (solid lines).

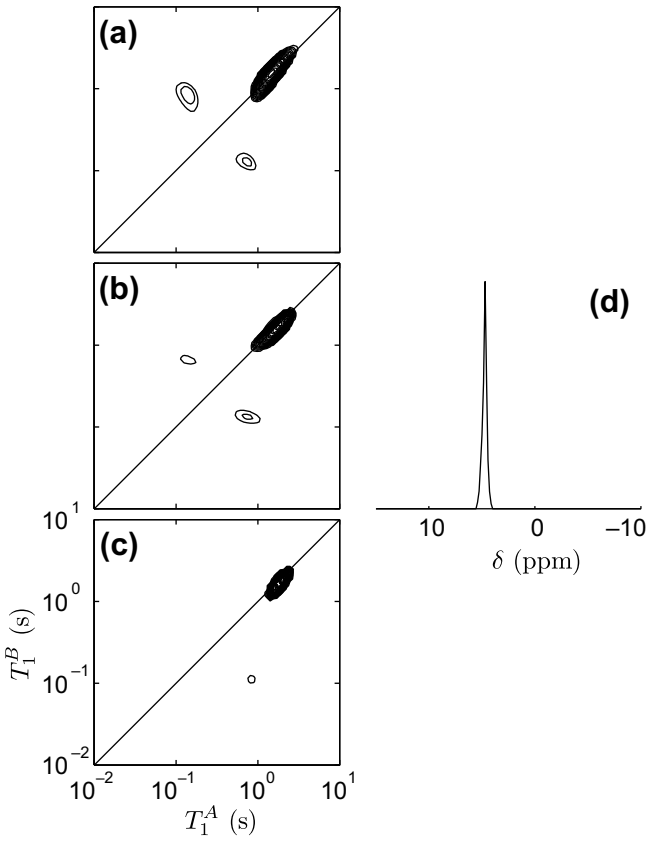


**Fig. 4.** $T_1$–$T_1$–$(\delta)$ exchange plots for water saturated cellulose fibres with exchange observation times of (a) $t_{ex} = 2$, (b) 32, and (c) 128 ms. The contour intervals are the same in each plot. (d) A typical spectrum from the last dimension of the $T_1$–$T_1$–$(\delta)$ data: only a single line is observed corresponding to water ($\delta = 4.69$ ppm, referenced to $CH_2$ at $\delta = 1.27$ ppm) and so the spectra were simply integrated to provide a two-dimensional data set.

sequence. This is akin to the observation of exchange peaks in $T_1$–$T_2$ correlations [25] where there is no defined exchange time interval. As the exchange time in the $T_1 - T_1$ experiment increases, the intensity of the exchange peaks $I_{XP}$ is seen to decrease (relative to the main peaks $I_{MP}$) due to a combination of $T_2$ relaxation and diffusive exchange. A $T_2$–$T_2$ exchange plot with $t_{ex} = 200$ ms is shown in Fig. 5 for comparison. The $T_2$–$T_2$ measurement is subtly different from the $T_1 - T_1$ measurement in that significant evolution of the exchange peaks is only observed over the longitudinal storage interval. In the $T_2$–$T_2$ plot it can be seen that the distribution is poorly resolved and that additional peaks are present, attributable to susceptibility artefacts. The $T_1$–$T_1$–$(\delta)$ measurement is unaffected by these internal gradients and distinct peaks are observed in Fig. 4. The $T_1$–$T_1$–$(\delta)$ exchange measurement also has the advantage of retaining chemical shifts—see Fig. 4(d), for example—although the additional information was not used in this case.

An average exchange time has been estimated from the $T_1$–$T_1$–$(\delta)$ exchange plots using the method proposed by Washburn and Callaghan [2]. A single component exponential decay was fitted to the ratio of exchange peak to main peak intensity $I_{XP}/I_{MP}$, see Fig. 6(a), to provide an effective exchange time $\tau_{ex}^{eff} = 66$ ms. The exponential decrease in the relaxation exchange peak intensity is governed by transverse relaxation and diffusive exchange during the exchange interval. The effective exchange time was corrected to account for the $T_2$ relaxation using

$$\frac{1}{\tau_{ex}} = \frac{1}{\tau_{ex}^{eff}} + \frac{1}{T_2}, \tag{2}$$

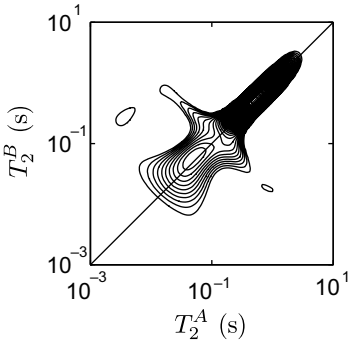


**Fig. 5.** Example of a $T_2$–$T_2$ exchange plot for water-saturated cotton fibres with an exchange observation time of $t_{ex} = 200$ ms. The main peaks are merged in a continuous distribution and several peaks can be seen either side of the $T_2^A = T_2^B$ line, making identification of the true exchange peaks difficult.

where $T_2 = 1.29$ s (determined from a one-dimensional CPMG measurement), to give an actual exchange time of $\tau_{ex} = 63$ ms $\pm$ 3 ms. This corresponds to an exchange distance of $R_X \approx 14$ μm, based on the bulk diffusion coefficient of water. This is comparable to the diameters of the fibres, estimated elsewhere to be on the order of 12–20 μm [27], or pores seen to be $\leqslant$20 μm in length extending along the axis of the fibres [28]. A similar exchange time of $\tau_{ex} = 54$ ms $\pm$ 20 ms was estimated from the $T_2$–$T_2$ exchange measurements (corrected for $T_1$ relaxation), see Fig. 6(b), where the relative exchange peak intensity is seen to increase because of

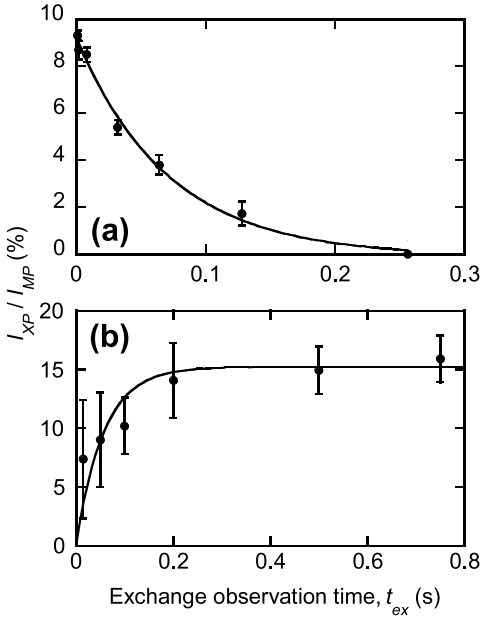


**Fig. 6.** Variation in exchange peak ($I_{XP}$) to main peak ($I_{MP}$) intensity as a function of exchange interval duration for (a) $T_1$–$T_1$–($\delta$) and (b) $T_2$–$T_2$ analysis of water in cotton fibres. In each plot the solid line represents a single-component exponential fit to the data.

longitudinal recovery throughout the exchange interval. The peak intensities were determined by integrating the appropriate peaks in the two-dimensional plots. The error bars in Fig. 6 were derived from the accuracy of the integration process: see [10,11] for further details. The errors are significantly larger in the $T_2$–$T_2$ experiment because the peaks are not resolved discretely and multiple off-diagonal peaks are present, complicating the analysis.

## 4. Conclusions

In this paper, we have demonstrated the ability to encode $T_1$ in the second dimension of two-dimensional relaxation correlation measurements in such a way as to retain chemical shift information without increasing the experimental time. Correspondingly, a $T_2$–$T_1$–$\delta$ correlation has been demonstrated whereby the signals arising from oil and water in a sandstone rock core were unambiguously separated. Since the fractions of surface relaxing oil and water can be determined, this analysis may provide a method of determining and quantifying the wettability of a rock core in a laboratory scale experiment. This addition to the suite of multi-dimensional NMR measurements is dependent on a rapid "double-shot" method of encoding $T_1$ with spectral resolution, validated here with a model system against the conventional inversion recovery method.

We have also demonstrated the feasibility of a novel $T_1$–$T_1$–($\delta$) relaxation exchange measurement. These experiments were seen to provide discrete exchange peaks for water in cellulose fibres. Conventional $T_2$–$T_2$ exchange measurements performed on the same sample provided two-dimensional distributions of relaxation times that did not exhibit discrete exchange peaks and were distorted by magnetic susceptibility artefacts. There are many other potential applications for these multi-dimensional relaxation correlations including biological cells [29], cement [25], liquid crystals [30], foods [9], and emulsions [31]. The addition of the chemical shift information means these correlations can be applied to a wider range of macroscopically heterogeneous systems.

## Acknowledgments

The authors thank Drs. Daniel Beauregard, Andy Sederman, and Dan Holland for helpful discussions. For financial support T.C.C. thanks Syngenta and J.M. thanks Schlumberger Cambridge Research.

## References

[1] Y.Q. Song, L. Venkataramanan, M.D. Hürlimann, M. Flaum, P. Frulla, C. Straley, $T_1$–$T_2$ correlation spectra obtained using a fast two-dimensional Laplace inversion, J. Magn. Reson. 154 (2) (2002) 261–268.
[2] K.E. Washburn, P.T. Callaghan, Tracking pore to pore exchange using relaxation exchange spectroscopy, Phys. Rev. Lett. 97 (17) (2006) 175502.
[3] H. Carr, E. Purcell, Effects of diffusion on free precession in NMR experiments, Phys. Rev. 94 (1954) 630–638.
[4] S. Meiboom, D. Gill, Modified spin-echo method for measuring nuclear relaxation times, Rev. Sci. Instrum. 29 (1958) 668–691.
[5] P.T. Callaghan, S. Godefroy, B.N. Ryland, Diffusion-relaxation correlation in simple pore structures, J. Magn. Reson. 162 (2) (2003) 320–327.
[6] M.D. Hürlimann, L. Venkataramanan, Quantitative measurement of two-dimensional distribution functions of diffusion and relaxation in grossly inhomogeneous fields, J. Magn. Reson. 157 (1) (2002) 31–42.
[7] M.D. Hürlimann, M. Flaum, L. Venkataramanan, C. Flaum, R. Freedman, G.J. Hirasaki, Diffusion–relaxation distribution functions of sedimentary rocks in different saturation states, Magn. Reson. Imaging 21 (3–4) (2003) 305–310.
[8] N. Marigheto, L. Venturi, D. Hibberd, K.M. Wright, G. Ferrante, B.P. Hills, Methods for peak assignment in low-resolution multidimensional NMR cross-correlation relaxometry, J. Magn. Reson. 187 (2) (2007) 327–342.
[9] S. Godefroy, L.K. Creamer, P.J. Watkinson, P.T. Callaghan, The use of 2D Laplace inversion in food material, in: P.S. Belton, A.M. Gil, G.A. Webb, D. Rutledge (Eds.), Magnetic Resonance in Food Science: Latest Developments, Cambridge, 2003, pp. 85–92.
[10] L. Monteilhet, J.P. Korb, J. Mitchell, P.J. McDonald, Observation of exchange of micropore water in cement pastes by two-dimensional $T_2$–$T_2$ nuclear magnetic resonance relaxometry, Phys. Rev. E 74 (6) (2006) 061404.
[11] J. Mitchell, J.D. Griffith, J.H.P. Collins, A.J. Sederman, L.F. Gladden, M.L. Johns, Validation of NMR relaxation exchange time measurements in porous media, J. Chem. Phys. 127 (23) (2007) 234701.
[12] D.C. Look, D.R. Locker, Time saving in measurement of NMR and EPR relaxation times, Rev. Sci. Instrum. 41 (2) (1970) 250–251.
[13] R. Grumann, H. Barfuß, H. Fischer, D. Hentschel, A. Oppelt, TOMROP: a sequence for determining the longitudinal relaxation time $T_1$ in magnetic resonance tomography, Electromedica 55 (1987) 67–72.
[14] R.L. Steever, H. Carr, Nuclear magnetic resonance of $Xe^{129}$ in natural xenon, Phys. Rev. 121 (1961) 20–25.
[15] P.B. Kingsley, Methods of measuring spin-lattice ($T_1$) relaxation times: An annotated bibliography, Concept. Magn. Reson. 11 (4) (1999) 243–276.
[16] M.D. Hürlimann, Encoding of diffusion and $T_1$ in the CPMG echo shape: Single-shot D and $T_1$ measurements in grossly inhomogeneous fields, J. Magn. Reson. 184 (1) (2007) 114–129.
[17] E.E. Sigmund, N. Caudal, Y.Q. Song, Rapid $T_1$ measurement via decay-recovery decomposition: applications in fringe field and distributed relaxation experiments, Solid State Nucl. Magn. Reson. 29 (1-3) (2006) 232–241.
[18] J.J. Hsu, I.J. Lowe, Spin-lattice relaxation and a fast $T_1$-map acquisition method in MRI with transient-state magnetization, J. Magn. Reson. 169 (2) (2004) 270–278.
[19] J.P. Stamps, B. Ottink, J.M. Visser, J.P.M. van Duynhoven, R. Hulst, Difftrain: a novel approach to a true spectroscopic single-scan diffusion measurement, J. Magn. Reson. 151 (1) (2001) 28–31.
[20] R. Vold, J. Waugh, M. Klein, D. Phelps, Measurement of spin relaxation in complex systems, J. Chem. Phys. 48 (1968) 3831–3832.
[21] F. Bloch, Nuclear induction, Phys. Rev. 70 (1946) 460–474.
[22] J.D. Wilson, Statistical approach to the solution of 1st-kind integral-equations arising in the study of materials and their properties, J. Mater. Sci. 27 (14) (1992) 3911–3924.
[23] L. Venkataramanan, Y.Q. Song, M.D. Hürlimann, Solving Fredholm integrals of the first kind with tensor product structure in 2 and 2.5 dimensions, IEEE Tans. Signal Process. 50 (5) (2002) 1017–1026.
[24] J.P. Butler, J.A. Reeds, S.V. Dawson, Estimating solutions of the first kind integral equations with nonnegative constraints and optimal smoothing, SIAM J. Numer. Anal. 18 (3) (1981) 381–397.
[25] P.J. McDonald, J.P. Korb, J. Mitchell, L. Monteilhet, Surface relaxation and chemical exchange in hydrating cement pastes: a two-dimensional NMR relaxation study, Phys. Rev. E 72 (1) (2005) 011409.
[26] V.I. Volkov, S.A. Korotchkova, I.A. Nesterov, H. Ohya, Q.H. Guo, J.C. Huang, J.A. Chen, The self-diffusion of water and ethanol in cellulose derivative membranes and particles with the pulsed field gradient NMR data, J. Membrane Sci. 110 (1) (1996) 1–11.
[27] S.M. Loffler, Dyeing of cellulose fibres: a case study in structure-transport relationships in heterogeneous porous media, Ph.D. Thesis, University of Cambridge, 1996.

[28] T.Q. Li, U. Henriksson, L. Ödberg, Determination of pore volume in cellulose fibres by the pulsed gradient spin-echo NMR technique, J. Colloid Interf. Sci. 169 (1995) 376–379.
[29] K.R. Brownstein, C.E. Tarr, Importance of classical diffusion in NMR studies of water in biological cells, Phys. Rev. A 19 (6) (1979) 2446–2453.
[30] P.T. Callaghan, I. Furo, Diffusion–diffusion correlation and exchange as a signature for local order and dynamics, J. Chem. Phys. 120 (8) (2004) 4032–4038.
[31] M.L. Johns, K.G. Hollingsworth, Characterisation of emulsion systems using NMR and MRI, Prog. Nucl. Magn. Reson. Spectrosc. 50 (2–3) (2007) 51–70.